The apical anion exchanger Slc26a6 promotes oxalate secretion by murine submandibular gland acinar cells

Received for publication, February 9, 2018, and in revised form, March 8, 2018 Published, Papers in Press, March 12, 2018, DOI 10.1074/jbc.RA118.002378

Taro Mukaibo[‡§1], Takashi Munemasa[‡§1], Alvin T. George[‡], Duy T. Tran[¶2], Xin Gao[‡‖], Jesse L. Herche[‡], Chihiro Masaki[§], Gary E. Shull[**], Manoocher Soleimani[‡‡], and James E. Melvin[‡3]

From the [‡]Secretory Mechanisms and Dysfunctions Section and [¶]Biological Chemistry Section, NIDCR, National Institutes of Health, Bethesda, Maryland 20892, the [§]Department of Oral Reconstruction and Rehabilitation, Kyushu Dental University, Kitakyushu, Fukuoka 803-8580, Japan, the [‖]Joint Institute for Food Safety and Applied Nutrition, University of Maryland, College Park, Maryland 20742, and the Departments of [‡‡]Medicine and [**]Molecular Genetics, Biochemistry, and Microbiology, University of Cincinnati College of Medicine, Cincinnati, Ohio 45267

Edited by Mike Shipston

The solute carrier family 26 (*SLC26*) gene family encodes at least 10 different anion exchangers. SLC26 member 6 (SLC26A6 or CFEX/PAT-1) and the cystic fibrosis transmembrane conductance regulator (CFTR) co-localize to the apical membrane of pancreatic duct cells, where they act in concert to drive HCO_3^- and fluid secretion. In contrast, in the small intestine, SLC26A6 serves as the major pathway for oxalate secretion. However, little is known about the function of Slc26a6 in murine salivary glands. Here, RNA sequencing–based transcriptional profiling and Western blots revealed that *Slc26a6* is highly expressed in mouse submandibular and sublingual salivary glands. Slc26a6 localized to the apical membrane of salivary gland acinar cells with no detectable immunostaining in the ducts. CHO-K1 cells transfected with mouse *Slc26a6* exchanged Cl^- for oxalate and HCO_3^-, whereas two other anion exchangers known to be expressed in salivary gland acinar cells, Slc4a4 and Slc4a9, mediated little, if any, Cl^-/oxalate exchange. Of note, both Cl^-/oxalate exchange and Cl^-/HCO_3^- exchange were significantly reduced in acinar cells isolated from the submandibular glands of *Slc26a6*$^{-/-}$ mice. Oxalate secretion in submandibular saliva also decreased significantly in *Slc26a6*$^{-/-}$ mice, but HCO_3^- secretion was unaffected. Taken together, our findings indicate that Slc26a6 is located at the apical membrane of salivary gland acinar cells, where it mediates Cl^-/oxalate exchange and plays a critical role in the secretion of oxalate into saliva.

The *SLC26* gene family encodes at least ten functionally diverse anion exchangers (SLC26A1–11), including SAT-1 (SLC26A1), DTDST (SLC26A2), DRA/CLD (SLC26A3), PDS/Pendrin (SLC26A4), PRES/Prestin (SLC26A5), CFEX/PAT-1 (SLC26A6), SUT2 (SLC26A7), SPGF3 (SLC26A8), and SLC26A9 and SLC26A11, and there is suggestive evidence that SLC26A10 may be a pseudogene in humans (1). SLC26 proteins transport numerous anions, such as HCO_3^-, OH^-, Cl^-, I^-, formate, oxalate, and sulfate (2–4). Although some members of the SLC26A family transport a limited number of specific substrates, SLC26A6 displays little anion selectivity (2, 5).

SLC26A6 has cytoplasmic N and C termini that flank an integral membrane domain containing 10 to 14 transmembrane segments as well as a sulfate transporter and anti-σ factor antagonist (STAS)[4] domain located in the C terminus. The STAS domain interacts with other ion transport proteins to form transport metabolons (1, 6–8). One proposed example of such an interaction is the mutual activation of CFTR and SLC26A6 in pancreatic duct cells, which depends on the physical association of the STAS domain of SLC26A6 with the R domain of CFTR (7). CFTR and SLC26A6 activation is apparently enhanced by protein kinase A (PKA)–mediated phosphorylation of the R domain (9).

SLC26A6 expression is ubiquitous, but it is highly expressed in the pancreas, small intestine, and kidney (10, 11). Transcriptional profiling also found that Slc26a6 is highly expressed in murine salivary glands (12). Targeted disruption of mouse *Slc26a6* inhibited HCO_3^- and fluid secretion in the pancreas (13), whereas oxalate secretion in the small intestine and reabsorption by the kidney were markedly reduced (14–17). These results suggest that Slc26a6 may play several crucial roles in mammalian physiology, *e.g.* secretion of fluid and HCO_3^- by the pancreas to neutralize stomach acid and secretion of oxalate by the intestine to regulate plasma oxalate levels and prevent kidney stone formation (15, 18–20).

The function of Slc26a6 in salivary glands is unclear, although it has been suggested that Slc26a6 contributes to fluid and HCO_3^- secretion, as demonstrated in the pancreas (21–24). Alternatively, Slc26a6 in salivary glands may play a role in the

This work was supported by National Institutes of Health Grant 1-ZIA-DE000738 (to J. E. M.). The authors declare that they have no conflicts of interest with the contents of this article. The content is solely the responsibility of the authors and does not necessarily represent the official views of the National Institutes of Health.

[1] Both authors contributed equally to this work.

[2] Supported by Grant 1-ZIA-DE000739 (to Lawrence A. Tabak) from the Intramural Research Program of the NIDCR, National Institutes of Health.

[3] To whom correspondence should be addressed. Tel.: 301-402-1706; E-mail: james.melvin@nih.gov.

[4] The abbreviations used are: STAS, sulfate transporter and anti-σ factor antagonist; CFTR, cystic fibrosis transmembrane conductance regulator; RNA-seq, RNA sequencing; PG, parotid gland; SMG, submandibular gland; SLG, sublingual gland; qPCR, quantitative PCR; FPKM, fragments per kilobase of transcript per million mapped reads; cDNA, complementary DNA; CHO, Chinese hamster ovary; CFEX, chloride/formate exchanger; BCECF, 2′,7′-bis-(2-carboxyethyl)-5-(and-6)-carboxyfluorescein; AM, acetoxymethyl ester; SPQ, 6-methoxy-*N*-(3-sulfopropyl) quinolimium; A01, T16Ainh-A01; EZA, ethoxzolamide; IPR, isoproterenol; BME, basal medium Eagle; ANOVA, analysis of variance; NMDG, *N*-methyl-D-glucamine.

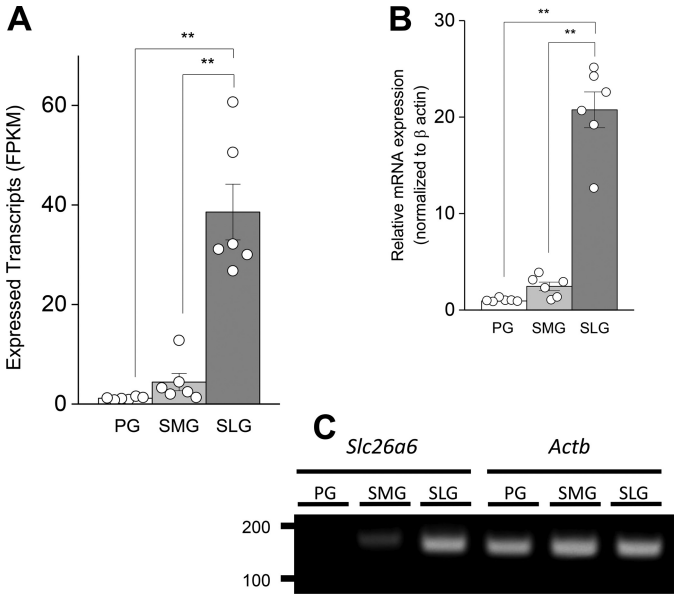

Figure 1. Slc26a6 mRNA expression in mouse salivary glands. *A*, *Slc26a6* expression acquired by RNA-seq analysis for mouse PGs, SMGs, and SLGs are displayed as FPKM per 40 million mapped reads. Data from individual glands are displayed as *circles* ($n = 6$ for PG, SMG, and SLG). *B*, *Slc26a6* mRNA expression levels were confirmed by qPCR and normalized to β-actin (*Actb*) ($n = 6$ for PG, SMG, and SLG). *C*, PCR band size and product amount for *slc26a6* (149 bp) and *Actb* (147 bp) after PCR 27 cycles of cDNA amplification (100 ng). One-way ANOVA followed by Bonferroni's *post hoc* test was performed for statistical analysis; **, $p < 0.01$.

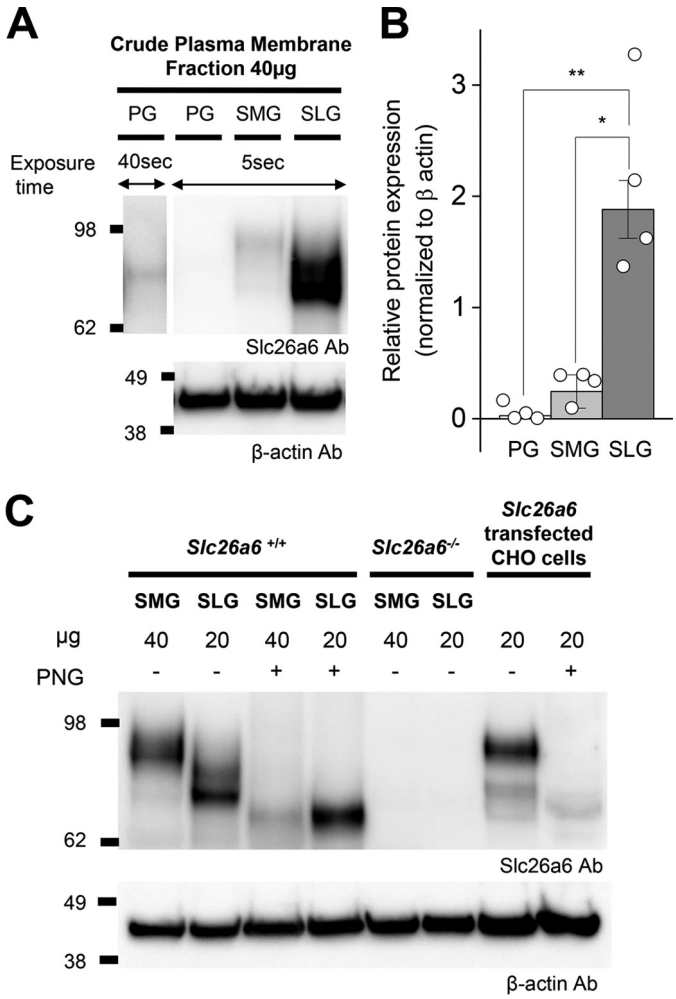

Figure 2. Slc26a6 protein expression in mouse salivary glands. *A*, crude plasma membrane was isolated from PGs, SMGs, and SLGs. Each lane was loaded with 40 μg of protein and immunoblotted with mouse monoclonal antibodies (*Ab*) to Slc26a6 and β-actin. To more clearly visualize Slc26a6 protein expression in PGs, the blot was developed for 40 s (*first lane*). *B*, band intensities from *A* were quantified using ImageJ software and normalized to β-actin ($n = 4$). One-way ANOVA followed by Bonferroni's *post hoc* test was performed for statistical analysis; *, $p < 0.002$, **, $p < 0.01$. *C*, SMG (40 μg) and SLG (20 μg) plasma membrane proteins from *Slc26a6*$^{+/+}$ and *Slc26a6*$^{-/-}$ mice and from *Slc26a6*-transfected CHO cells (20 μg) were treated without (−) or with (+) PNGaseF (*PNG*). The same membrane as in *A* was stripped and immunoblotted with an anti-β-actin antibody ($n = 3$).

secretion of oxalate, as in the small intestine (16). In fact, oxalate has been detected in human saliva and sialolithes (25, 26), where it might contribute to salivary gland stone formation.

Thus, the aim of this study is to test, in murine salivary glands, two major hypotheses: Slc26a6 functions predominantly as a Cl^-/HCO_3^- exchanger and contributes to HCO_3^- secretion and/or Slc26a6 largely functions in Cl^-/oxalate exchange mode and thus plays a critical role in oxalate secretion. Our results suggest, in contrast to the pancreas, that Slc26a6 does not target to the apical membrane of duct cells, nor does it promote HCO_3^- secretion. Instead, Slc26a6 localizes to the apical membrane of salivary gland acinar cells, where it appears to play a major role in oxalate secretion.

Results

Slc26a6 mRNA is expressed in murine salivary glands

RNA-seq data were acquired and described previously (12), and the full data sets were deposited in the Gene Expression Omnibus (GEO accession number GSE96747). Further analysis of these data revealed *Slc26a6* transcript expression in the major salivary glands, the parotid gland (PG), submandibular gland (SMG), and sublingual (SLG) gland. SLG *Slc26a6* expression exceeded the levels found in the PG and SMG by ~33- and 9-fold, respectively (Fig. 1*A*). Validation by qPCR analysis showed that the relative expression of *Slc26a6* mRNA in the SLG was 22- and 9-fold greater than in the PG and SMG, respectively (Fig. 1*B*), comparable with the RNA-seq data. *Slc26a6* mRNA expression was normalized to the β-actin housekeeping gene *Actb* (Fig. 1*C*), whose expression, as resolved by RNA-seq, was not significantly different in the PG, SMG, and SLG (mean FPKM ± S.E. = 403.5 ± 27.3, 503.5 ± 93.3, and 553.3 ± 82.6, respectively; $n = 6$ for each gland). This was also confirmed by qPCR analysis, where the Cq values for β-actin were 20.8 ± 0.5, 19.4 ± 0.6, and 19.1 ± 0.3 for the PG, SMG, and SLG, respectively ($n = 6$ for each gland).

Slc26a6 is modified by N-linked glycosylation

To examine Slc26a6 protein expression across the three major murine salivary glands, 40 μg of plasma membrane protein from each gland was separated by SDS-PAGE followed by Western blotting. Consistent with Slc26a6 mRNA expression levels, the protein expression level in the SLG was ~39- and 7-fold higher than in the PG and SMG, respectively (Fig. 2, *A* and *B*). Little Slc26a6 protein was detectable above background in the PG lane when the exposure time was only 5 s, but it was clearly visible when developed for 40 s (Fig. 2*A*, *first lane*).

The protein band detected in the SLG lane ran ~10–15 kDa smaller compared with the plasma membrane protein isolated

from the SMG and from *Slc26a6* cDNA-transfected CHO cells (Fig. 2*C*). It was reported previously that human and mouse SLC26A6 are heavily *N*-glycosylated in a tissue-specific manner (27). Correspondingly, treatment with the *N*-linkage–specific glycosidase PNGaseF resulted in a shift to a similar molecular mass of ~70–80 kDa in SMG, SLG and *Slc26a6* pcDNA transfected CHO cells, suggesting that the smaller apparent size of Slc26a6 in the SLG is caused by less *N*-glycosylation modification (Fig. 2*C*) and not gland-specific differences in alternative splicing of the Slc26a6 transcript. Indeed, a comparison of the salivary gland transcriptomes revealed that the 18 exons comprising the *Slc26a6* gene, including predicted *N*-glycosylation sites at asparagine 151 and 303 (http://www.cbs.dtu.dk/services/NetNGlyc/),[5] are expressed in the PG, SMG, and SLG (12). Note that the predicted unmodified protein molecular mass of mouse Slc26a6 is ~83 kDa (UniportKB Q8CIW6-1).

Furthermore, comparison of SMG and SLG transcriptomes failed to detect major differences in the expression of genes involved in *N*-glycosylation of Slc26a6 (28), *e.g.* the 12 members of the *Alg* gene family of glucosyltransferases, except for *Alg8*. Although called significantly different by bioinformatics analysis (Cufflinks/Cuffdiff 2.2.1), *Alg8* expression in the SMG was only about 40% less than that detected in the SLG (FPKM = 5.76 and 9.79, respectively; $q < 0.026$; $n = 6$ for each gland type). Thus, the expression patterns of glucosyltransferase genes do not easily explain the large differences in *N*-glycosylation of Slc26a6 in the SMG and SLG, suggesting that it likely involves differences in expression of genes that add other moieties to the oligosaccharide structure and/or signaling pathways that regulate translation of Alg mRNAs and glucosyltransferase activity.

Slc26a6 localizes to the apical membrane of salivary gland acinar cells

Previous reports suggest that Slc26a6 is localized to the apical membrane of epithelial tissues, including the duct cells of the pancreas (21, 29), small intestine, and kidney proximal tubules (11, 30, 31), where it is thought to regulate pancreatic HCO_3^- secretion and intestinal and renal oxalate transport (20, 32, 33). Thus, immunohistochemistry was performed to better understand the functional targeting of Slc26a6 in the SMG, SLG, and PG of WT mice (*Slc26a6*$^{+/+}$). Strong immunostaining of Slc26a6 (Fig. 3, *cyan*, *open white arrows*) was detected at the apical membranes of SMG and SLG acinar cells (Fig. 3, *A* and *B*, and Fig. 3, *D* and *E*, respectively), whereas Nkcc1-specific antibody (Fig. 3, *red*, *filled red arrows*) labeled the basolateral membranes of acinar cells and Cftr-specific antibody (Fig. 3, *green*, *filled white arrows*) stained the apical membranes of duct cells. In contrast, considerably less Slc26a6 staining was detected in the PG of WT mice, consistent with lower expression of Slc26a6 in this gland (data not shown).

Immunostaining of Slc26a6 in the SMG and SLG was negative in *Slc26a6*$^{-/-}$ mice, verifying the specificity of the anti-Slc26a6 antibody (Fig. 3, *C* and *F*), whereas Nkcc1 staining (Fig. 3, *filled red arrow*) was unaffected in the basolateral membranes of acinar cells in *Slc26a6*$^{-/-}$ mice.

[5] Please note that the JBC is not responsible for the long-term archiving and maintenance of this site or any other third party–hosted site.

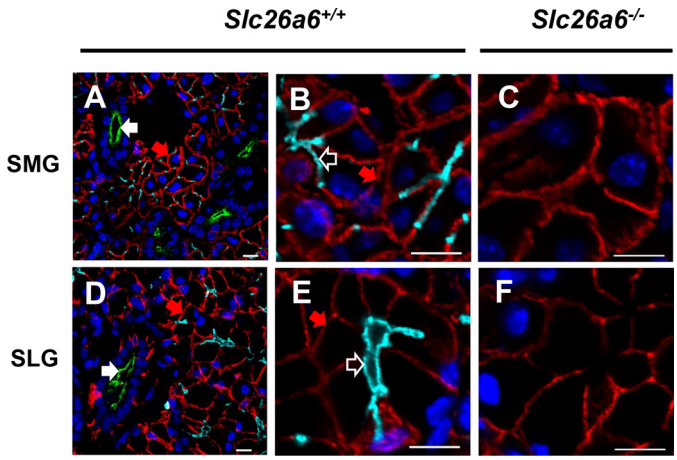

Figure 3. Slc26a6 localizes to the apical membranes of mouse salivary gland acinar cells. Shown is immunofluorescent staining of Slc26a6 (*cyan*), Cftr (*green*), and Nkcc1 (*red*). Nuclei were stained with 4′,6-diamidino-2-phenylindole (*blue*). *A*, Slc26a6 localized at the apical membrane of SMG acinar cells from *Slc26a6*$^{+/+}$ mice, with no overlap of apical duct Cftr (*filled white arrow*) or basolateral acinar Nkcc1 (*filled red arrow*) staining. *B*, high magnification image of Slc26a6 staining of the acinar cell apical membrane (*open white arrow*) from *A*. *C*, Slc26a6 was not detected in the SMGs of *Slc26a6*$^{-/-}$ mice, whereas Nkcc1 staining was unchanged. *D* and *E*, Slc26a6 localized at the apical membrane of SLG acinar cells from *Slc26a6*$^{+/+}$ mice, with no Cftr or Nkcc1 overlap. *F*, Slc26a6 was not detected in the SMGs of *Slc26a6*$^{-/-}$ mice, whereas Nkcc1 staining was unchanged. Representative images of three independent experiments are shown. *Scale bars* = 10 μm.

Slc26a6 exchanges Cl^- for oxalate in transfected CHO-K1 cells

Slc26a6 (also known as CFEX, chloride/formate exchanger) was initially reported to exchange Cl^- for formate (5), but Slc26a6 was subsequently recognized to also transport other anions, such as oxalate and HCO_3^- (4). The above results demonstrated that Slc26a6 is exclusively expressed in salivary gland acinar cells; however, these cells also express the anion exchangers Ae2 (Slc4a2) and Ae4 (Slc4a9) (34, 35), which complicates the interpretation of studies to quantify Slc26a6-mediated anion exchange. Consequently, to verify that Slc26a6 oxalate transport activity can be isolated in salivary gland acinar cells, mouse *Slc26a6*, *Slc4a2*, and *Slc4a9* cDNAs were expressed in CHO-K1 cells, and Cl^-/oxalate exchange was monitored.

Oxalate-dependent Cl^- uptake (anion exchanger activity) was monitored in CHO-K1 cells with the intracellular Cl^- indicator SPQ under HCO_3^--free conditions as described under "Experimental procedures." Slc26a6-expressing CHO-K1 cells mediated Cl^-/oxalate exchange (Fig. 4*A*, results summarized in Fig. 4*B*). In contrast, Slc4a2- and Slc4a9-expressing CHO-K1 cells displayed little, if any, oxalate-dependent Cl^- uptake (Cl^-/oxalate exchanger activity). Thus, Cl^-/oxalate exchange can isolate Slc26a6 anion transport activity from the other known anion exchangers expressed in salivary gland acinar cells.

Slc26a6 mediates Cl^-/oxalate exchange in salivary gland acinar cells

Mouse SMG acinar cells were treated as above (Fig. 4) to induce Slc26a6-mediated Cl^-/oxalate anion exchange. To further isolate the Slc26a6-mediated Cl^-/oxalate exchange activity, Cl^- fluxes via the Ca^{2+}-activated anion channel Tmem16A and the $Na^+/K^+/2Cl^-$ cotransporter Nkcc1 were prevented

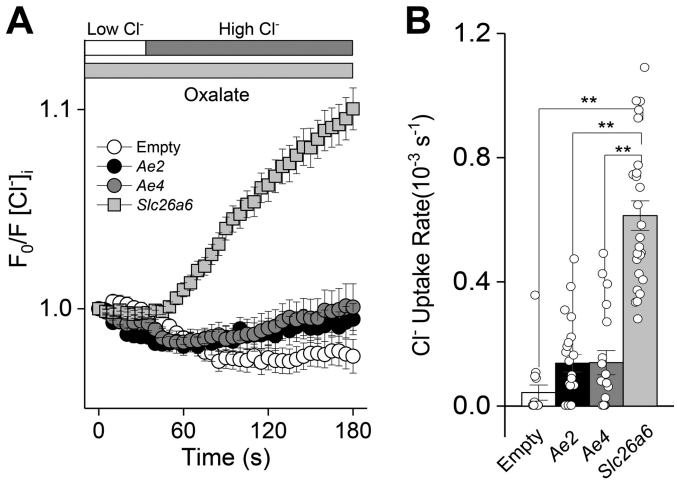

Figure 4. Oxalate-dependent Cl^- uptake by mouse *Slc26a6* in transfected CHO-K1 cells. CHO-K1 cells were transfected with plasmids containing either mouse *Slc26a6*, *Ae2* (*Slc4a2*), or *Ae4* (*Slc4a9*) cDNA, and the intracellular Cl^- concentration was measured using the Cl^--sensitive indicator SPQ. Intracellular Cl^- was initially depleting by exposure to a low Cl^- external solution, and then oxalate-dependent Cl^- uptake was induced by reintroduction of a high Cl^- solution. *A*, the high Cl^- solution induced little, if any, oxalate-dependent Cl^- uptake in *Ae2*-expressing (*black circles*, $n = 26$) or *Ae4*-expressing (*gray circles*, $n = 18$) CHO-K1 cells, whereas *Slc26a6*-transfected (*gray squares*, $n = 26$) CHO-K1 cells exhibited oxalate-dependent Cl^- uptake. Empty vector–transfected CHO cell did not induce Cl^- uptake (*Empty*, *white circles*, $n = 15$). *B*, summary of Cl^- uptake rates in the presence of oxalate. Data are presented as the mean ± S.E. of at least five cells per experiment from at least three different transfections. One-way ANOVA followed by Bonferroni's *post hoc* test was performed for statistical analysis; **, $p < 0.01$.

with the specific inhibitors T16Ainh-A01 (A01) and bumetanide, respectively, whereas Cl^-/HCO_3^- exchanger activity was eliminated with the carbonic anhydrase inhibitor ethoxzolamide (EZA) under HCO_3^--free conditions.

No Cl^- uptake was observed in the absence of oxalate in *Slc26a6*$^{+/+}$ SMG acinar cells, confirming that Cl^- uptake under these conditions represents Cl^-/oxalate exchange activity (Fig. 5*A*). Furthermore, Cl^- uptake was abolished in *Slc26a6*$^{-/-}$ mice (Fig. 5*B*), indicating that Slc26a6 is the primary mediator of Cl^-/oxalate exchange across the plasma membrane of SMG acinar cells. The results shown in Fig. 5, *A* and *B*, are summarized in Fig. 5*C*.

Slc26a6-dependent oxalate secretion in saliva

The above results demonstrate that Slc26a6 is localized to the apical membrane of salivary gland acinar cells, where it exchanges Cl^- for oxalate. We next tested whether Slc26a6 transport activity contributes to secretion of oxalate in saliva using the *ex vivo* mouse SMG. Submandibular glands were stimulated by perfusion with the β-adrenergic receptor agonist isoproterenol (IPR, 1 μM) under oxalate-containing (1 mM) and oxalate-free conditions. Fig. 6*A* shows that the salivary flow rate was unaffected by disruption of *Slc26a6* (*filled circles*, *Slc26a6*$^{-/-}$) or by the presence of oxalate in the perfusate. In contrast, the SMG of *Slc26a6*$^{-/-}$ mice secreted significantly less oxalate compared with *Slc26a6*$^{+/+}$ mice in the presence of oxalate, whereas there was no difference in the oxalate concentration of saliva from *Slc26a6*$^{+/+}$ and *Slc26a6*$^{-/-}$ mice in the oxalate-free perfusion solution (Fig. 6*B*). A summary of the net oxalate transport (oxalate concentration in oxalate-containing solution minus oxalate-free solution) for each gland is shown in Fig. 6*C*. These results show that Slc26a6 does not support fluid secretion but that Slc26a6 significantly contributes to oxalate secretion in the intact mouse SMG organ system.

To confirm the results obtained using the colorimetric oxalate assay, ion exchange chromatography was performed. SMG saliva was stimulated by IPR in the *ex vivo* perfusion system under oxalate-free conditions as describe above. The SMG saliva samples collected from *Slc26a6*$^{+/+}$ and *Slc26a6*$^{-/-}$ mice were then assayed for oxalate content by both assay methods (*Slc26a6*$^{+/+}$, colorimetric = 0.21 ± 0.01 mM, ion exchange chromatography = 0.19 ± 0.02 mM; *Slc26a6*$^{-/-}$, colorimetric = 0.17 ± 0.04 mM, ion exchange chromatography = 0.21 ± 0.02 mM; $n = 8$ for each group). There were no significant differences between assay methods or animal groups. Note that this experiment was performed in the absence of oxalate, indicating that salivary glands secrete endogenously generated oxalate. Moreover, there was no difference between *Slc26a6*$^{+/+}$ and *Slc26a6*$^{-/-}$ mice, suggesting the existence of additional unknown oxalate transport pathways.

Slc26a6 Disruption fails to alter HCO_3^- secretion

It has been reported that Slc26a6 and Cftr co-express in the apical membrane of pancreatic duct cells, where they act in concert to drive HCO_3^- and fluid secretion (13, 36), and that this interaction may also be important in salivary gland ducts (37, 38). However, Fig. 3 clearly demonstrates that Slc26a6 is expressed in mouse salivary gland acinar cells, whereas Cftr is found in the ducts. Moreover, disruption of *Slc26a6* had no effect on fluid secretion in the SMG (Fig. 6*A*).

To explore whether Slc26a6 contributes to salivary gland HCO_3^- secretion, we monitored the Cl^-/HCO_3^- exchange activity of SMG acinar cells loaded with the pH-sensitive indicator BCECF. Fig. 7*A* shows that Cl^-/HCO_3^- exchange activity was significantly reduced in acinar cells from *Slc26a6*$^{-/-}$ mice. Fig. 7*B* summarizes the alkalization rates for the results shown in Fig. 7*A* (*B*+) and also demonstrates that the alkalization induced by removal of extracellular Cl^- was HCO_3^--dependent (*B*−). In contrast to Cl^-/HCO_3^- exchange, the kinetics and magnitude of fluid secretion in response to the β-adrenergic receptor agonist (1 μM isoproterenol, IPR) were not altered in the SMG of *Slc26a6*$^{-/-}$ mice (Fig. 7*C*, similar to Fig. 6*A*). Moreover, the HCO_3^- concentration of saliva was comparable in *Slc26a6*$^{+/+}$ and *Slc26a6*$^{-/-}$ mice (Fig. 7*D*), suggesting that Slc26a6-mediated Cl^-/HCO_3^- exchange does not appreciably contribute to HCO_3^- secretion by the SMG.

Note that Slc26a6 mediated both Cl^-/oxalate and Cl^-/HCO_3^- exchange in SMG acinar cells. Consequently, it seems incongruous that Slc26a6 does not contribute to HCO_3^- secretion, whereas oxalate secretion was markedly reduced in *Slc26a6*$^{-/-}$ mice. However, Slc26a6 is the dominant oxalate transporter in SMG acinar cells, whereas it is but one of several HCO_3^- transport pathways in salivary glands. Indeed, in response to IPR stimulation, the SMG secretes ≤0.5 mM oxalate in contrast to about 80 mM HCO_3^-. We speculate that the contribution of Slc26a6-mediated Cl^-/HCO_3^- exchange to total HCO_3^- secretion is likely to be inconsequential compared with Na^+/HCO_3^- cotransporters, HCO_3^--permeant anion channels,

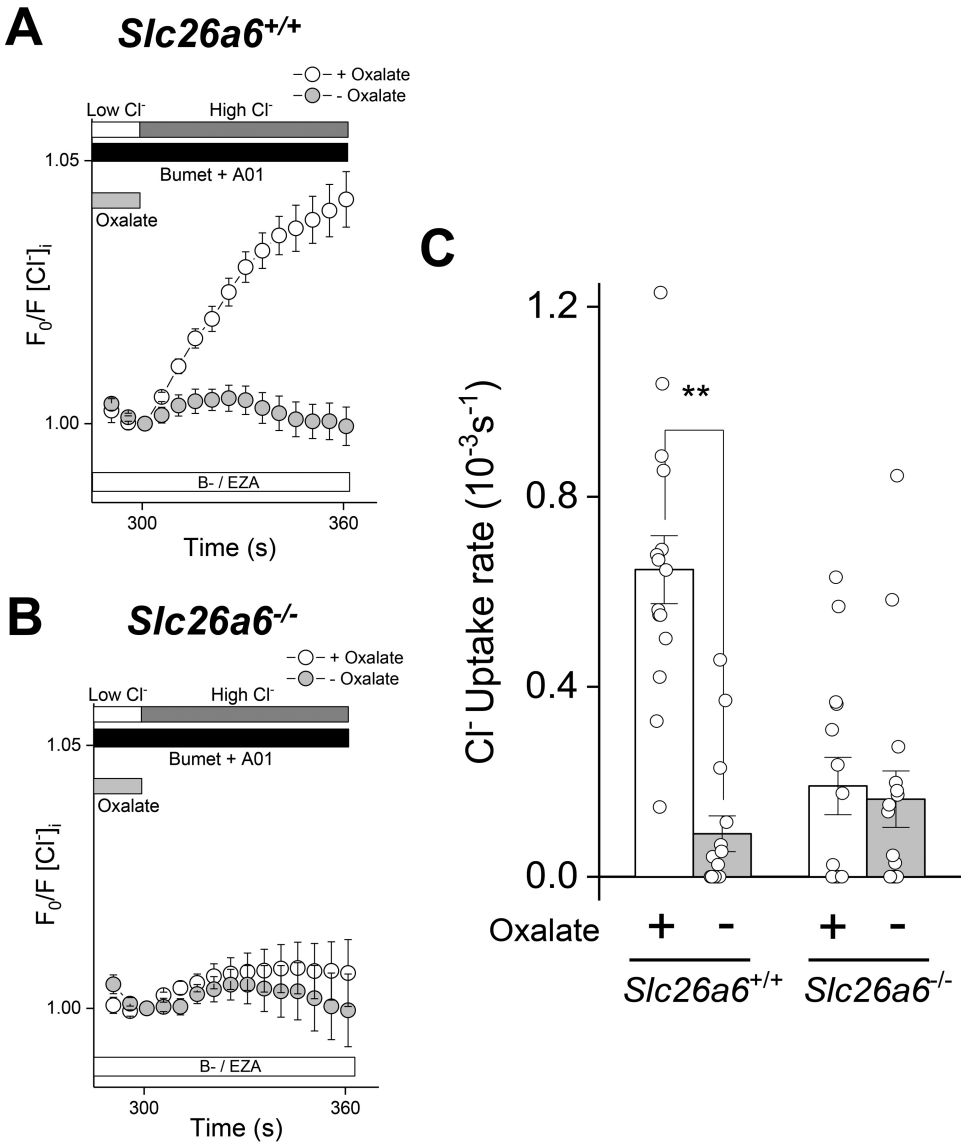

Figure 5. Slc26a6 mediates Cl^-/oxalate exchange in mouse SMG acinar cells. Acinar cells isolated from *Slc26a6*$^{+/+}$ and *Slc26a6*$^{-/-}$ submandibular glands were loaded with SPQ to monitor Cl^- uptake. Cl^- depletion was induced by incubation in a low Cl^- solution in the absence (− *Oxalate*) or presence (+ *Oxalate*) of 25 mM oxalate, and then Cl^- uptake was stimulated by reintroduction of high extracellular Cl^- in the absence of oxalate. Experiments were performed in bicarbonate-free solutions containing ethoxyzolamide (30 μM B−/EZA) to eliminate Cl^-/HCO_3^- exchange and T16Ainh-01 (10 μM A01) and bumetanide (*Bumet*, 80 μM) to inhibit Tmem16a and Nkcc1, respectively. *A*, oxalate-dependent Cl^- uptake was observed in *Slc26a6*$^{+/+}$ SMG acinar cells, but no Cl^- uptake was observed when oxalate was absent (+ *Oxalate*, *open circles*, $n = 15$; − *Oxalate*, *closed circles*, $n = 15$). *B*, Cl^-/oxalate exchange activity was absent in SMG acinar cells from *Slc26a6*$^{-/-}$ mice (+ *Oxalate*, *open circles*, $n = 14$; − *Oxalate*, *closed circles*, $n = 16$). *C*, summary of the Cl^- uptake experiments shown in *A* and *B*. Data are presented as the mean ± S.E. of cells isolated from at least four different mice per group. Statistical analysis was performed using unpaired *t* test; **, $p < 0.01$.

and the other Cl^-/HCO_3^- exchangers expressed in salivary gland acinar and duct cells, which both contribute to HCO_3^- secretion.

Discussion

The function of Slc26a6 in salivary glands is unknown, but Slc26a6 can function in multiple ion exchange modes, including Cl^-/oxalate exchange and Cl^-/HCO_3^- exchange in various tissues, such as kidney proximal tubule and small intestine (17). In the kidney proximal convoluted tubule, encompassing S1 and S2 segments, Slc26a6 predominantly functions in Cl^-/oxalate exchange mode (39), which, in parallel with SO_4^{2-}/oxalate exchange and Na^+-SO_4^{2-} cotransport, recycles the oxalate back, thus allowing a small concentration of oxalate to spur (drive up) chloride reabsorption (40). In the straight segment of the kidney proximal tubule (also known as the S3 segment), Slc26a6 predominantly functions in Cl^-/HCO_3^- exchange mode (39).

In the apical membrane of pancreatic duct cells, Slc26a6 acts as a Cl^-/HCO_3^- exchanger, where it co-expresses and is physically and functionally linked with the cAMP-activated Cl^- channel Cftr to drive HCO_3^- and fluid secretion (13). However, immunofluorescent staining showed that Slc26a6 targets to the apical membrane of salivary gland acinar cells, and thus, Slc26a6 clearly does not co-localize with Cftr in salivary gland duct cells. Functionally, these results demonstrate that salivary

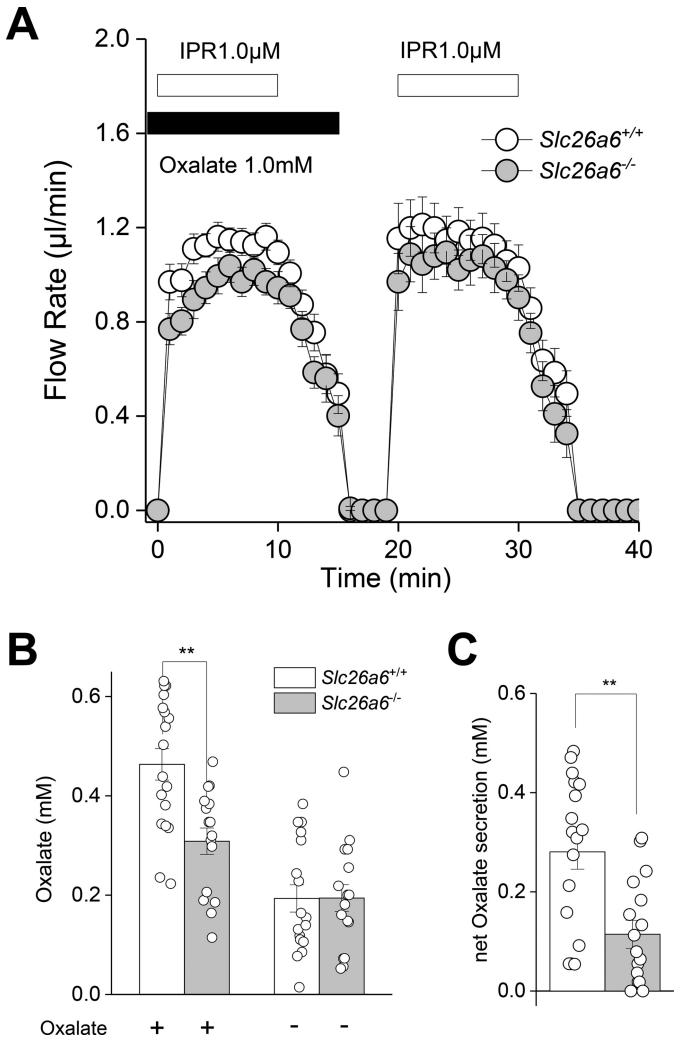

Figure 6. Slc26a6 mediates oxalate secretion in response to β-adrenergic receptor stimulation. The *ex vivo* SMG was perfused in the presence (1 mM) or absence of oxalate and subsequently stimulated with the β-adrenergic receptor agonist IPR (1.0 μM) to induce saliva secretion. *A*, flow rate and flow amount (microliters) were comparable in *Slc26a6*$^{+/+}$ (n = 26) and *Slc26a6*$^{-/-}$ (n = 23) mice. *B*, the oxalate concentration in saliva induced in the presence of oxalate was significantly less in *Slc26a6*$^{-/-}$ mice, whereas the oxalate concentration in the oxalate-free solution was comparable for *Slc26a6*$^{+/+}$ (n = 17) and *Slc26a6*$^{-/-}$ (n = 16) mice. *C*, net oxalate concentration = (oxalate concentration in oxalate-containing solution) minus (oxalate concentration in oxalate-free solution), subtracted from consecutive stimulations within an individual gland. Paired Student's *t* test was performed; **, $p < 0.001$. Results are given as the mean ± S.E.

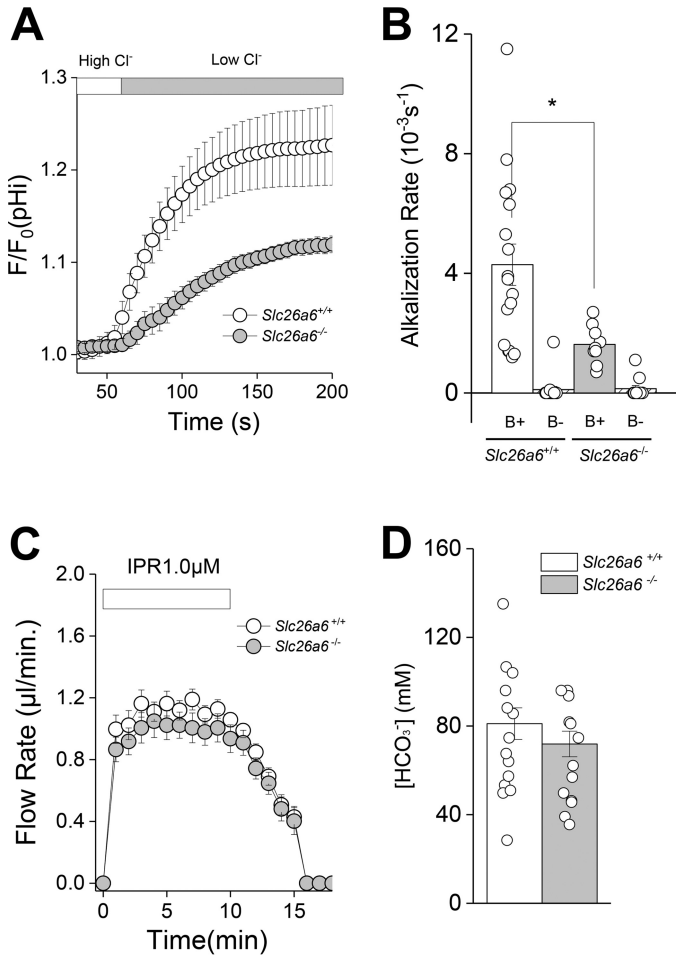

Figure 7. Acinar Cl^-/HCO_3^- exchanger activity and isoproterenol-induced HCO_3^- secretion in SMGs from *Slc26a6*$^{-/-}$ mice. *A*, intracellular alkalization was induced by Cl^-/HCO_3^- exchange in SMG acinar cells loaded with the pH indicator BCECF by shifting from a high Cl^- to a low Cl^- bath solution in the presence of HCO_3^- (*open circles*, *Slc26a6*$^{+/+}$; *closed circles*, *Slc26a6*$^{-/-}$). *B*, summary of the alkalization rates from the data in *A* (*B*+) and in HCO_3^--free (*B*−) solutions. The alkalization rate in the presence of HCO_3^- was significantly reduced in *Slc26a6*$^{-/-}$ SMG acinar cells (*Slc26a6*$^{+/+}$, B+ n = 17; *Slc26a6*$^{-/-}$, B+ n = 9), whereas alkalization was essentially eliminated under HCO_3^--free conditions (*Slc26a6*$^{+/+}$, B− n = 16; *Slc26a6*$^{-/-}$, B− n = 11). *C*, an *ex vivo* SMG was perfused with a 25 mM HCO_3^-- containing solution and stimulated with the β-adrenergic receptor agonist IPR (1.0 μM). Flow rate and flow amount (microliters) were comparable in *Slc26a6*$^{+/+}$ (n = 22) and *Slc26a6*$^{-/-}$ (n = 23) mice. *D*, bicarbonate concentration in saliva from *Slc26a6*$^{+/+}$ and *Slc26a6*$^{-/-}$ mice were comparable (*Slc26a6*$^{+/+}$, n = 14; *Slc26a6*$^{-/-}$, n = 13). Unpaired Student's *t* test was performed; *, $p < 0.05$. Results are given as mean ± S.E.

glands are quite different from the exocrine pancreas (21, 29). Indeed, Slc26a6 seems to contribute little, if at all, to either HCO_3^- or fluid secretion in salivary glands.

So what is the function of Slc26a6 in salivary glands? The role of Slc26a6 in salivary glands appears to mimic its role in the ileum with respect to oxalate. Slc26a6 shows strong expression along the length of small intestine, including the duodenum, jejunum, and ileum (11). In the duodenum, Slc26a6 functions predominantly as a Cl^-/HCO_3^- exchanger (39), whereas in the jejunum, Slc26a6, along with Slc26a3, plays critical roles in salt absorption, with Slc26a6 exhibiting enhanced activation by luminal fructose (41). In the ileum, Slc26a6 predominantly functions in Cl^-/oxalate exchange and plays a critical role in systemic oxalate homeostasis by exchanging the intracellular oxalate for luminal chloride (16). The net oxalate transport in the ileum favors oxalate secretion under baseline conditions (secretion > absorption); deletion of *Slc26a6* abrogates oxalate secretion, thus leaving the oxalate absorption pathway uncontested in the intestine, resulting in increased blood oxalate concentration with subsequent enhanced urine oxalate excretion (16) and kidney oxalate stone formation (19). It has been suggested that urolithiasis and sialolithes may be linked (42, 43). Indeed, oxalate is secreted in human saliva (44) and is detected in sialolithes (25, 26). Accordingly, we found that Cl^-/oxalate exchanger activity in the apical membrane of salivary gland acinar cells was eliminated in *Slc26a6*$^{-/-}$ mice. Consistent with acinar Slc26a6 playing a major role in the secretion of salivary oxalate, the concentration of oxalate in the saliva of *Slc26a6*$^{-/-}$ mice was markedly reduced.

The functional importance of oxalate in saliva remains to be determined, but one possibility is that insoluble calcium oxalate crystals deposit on the surface of the teeth, where it protects tooth enamel from the acid formed by oral bacteria following carbohydrate ingestion. Consistent with this model, oxalate is found on tooth enamel in various animals (44), whereas oxalic acid applied to teeth forms crystals and acts as a sealant on the enamel surface of the teeth (45). In addition to its physiological role on tooth enamel, it is noteworthy that oxalate is detectable in salivary stones (25, 26), suggesting that, under some conditions, Slc26a6-mediated oxalate secretion may contribute to sialolithiasis.

Experimental procedures

Materials and animals

Gene targeting and genotyping protocols for *Slc26a6*$^{-/-}$ mice were as described previously (39). *Slc26a6*$^{-/-}$ mice were backcrossed onto the FVB/NJ mouse background (The Jackson Laboratory). Mice were housed in micro-isolator cages with *ad libitum* access to laboratory chow and water during 12-h light/dark cycles. *Slc26a6*$^{+/+}$ littermates, or in some cases FVB/NJ mice (The Jackson Laboratory, stock no. 001800), were used as WT controls. Experiments were performed on approximately equal numbers of 2- to 4-month-old male and female mice. Mice were euthanized by inhalation of 100% CO_2, followed by cervical dislocation. All animal procedures were approved by the Animal Care and Use Committee of the NIDCR, National Institutes of Health (ASP 16-802). Reagents were purchased from Sigma-Aldrich (St. Louis, MO) unless otherwise indicated.

RNA sequencing analysis

RNA sequencing data were acquired as described previously (12). In brief, the PG, SMG, and SLG were surgically removed from six adult mice. The total RNA of the 18 glands was extracted, followed by cDNA synthesis and fragmentation to make Illumina libraries. The libraries were applied to Illumina HiSeq2500 sequencing, and the 18 sample libraries each had ~40 million reads. The data were put out as fragments per kilobase of transcript per million mapped reads (FPKM) values.

Validation of RNA-seq by quantitative PCR (qPCR)

The PG, SMG, and SLG from *Slc26a6*$^{+/+}$ and *Slc26a6*$^{-/-}$ littermates (three males and three females for each group, 8–12 weeks old) were removed with the aid of a dissecting microscope, immediately frozen in liquid nitrogen, and stored at −80 °C until shipping to MyOmicsDx (Towson, MD) for processing. Total RNA from each tissue was isolated using the MyGene^{TM}-RNA-EX kit, and 1 μg was reverse-transcribed to synthesize cDNA (MyGene^{TM}-RNA-RT kit). For negative controls, all components, except the reverse transcriptase, were included in the reaction mixtures. Real-time PCR was performed using the Bio-Rad CFX96 Touch^{TM} real-time PCR detection system with specific primers and the MyGene^{TM} qPCR master kit. PCR specificity was verified by the dissociation curve from a single peak, which was run following the real-time PCR reaction. The $2^{(-\Delta\Delta Cq)}$ (Livak) method was used to analyze the expression -fold change, and message levels were normalized to the abundance of β-actin messages. The primer sets were as follows: Slc26a6 mRNA, exon 1–2, forward 5′-AGATCTTCCTTGCGTCTGC-3′ and reverse 5′-GCCTTTCCACATGGTAGTCTC-3′, amplicon length 149 bp; Actb mRNA, exon 3–4, forward 5′-ACCTTCTACAATGAGCTGCG-3′ and reverse 5′-CTGGATGGCTACGTACATGG-3′, amplicon length 147bp. The PCR protocol was 1 min at 95 °C, 40 cycles of 15 s at 95 °C, and 30 s at 65 °C. Amplified products were visualized in 1.6% agarose gels in TAE (Tris-acetate buffer and EDTA). qPCR reactions were repeated three times for each sample and averaged to determine the expression -fold change.

Protein isolation and Western blot analysis

The crude plasma membrane protein fraction was isolated essentially as described previously (46). Briefly, mouse PGs, SMGs, and SLGs were removed, minced with fine scissors, and incubated in basal medium Eagle (BME) containing 1.0 mg/ml collagenase 2 (Worthington) with two steps of 25-min incubation at 37 °C. The dispersed cells were subsequently passed through a 150-μm cell strainer (Thermo Fisher), centrifuged in a clinical tabletop centrifuge for 1 min, and resuspended in lysate buffer containing 0.5% Igepal CA-630, 10 mM HEPES (pH 7.2 for the PG and SMG and pH 6.8 for the SLG), 0.3 M sucrose, 2 mM EDTA, 0.2 mM EGTA, 1 mM PMSF, and phosphatase and protease inhibitor mixtures (Roche). Lysed cells were centrifuged at 4000 × *g* for 10 min, and the supernatant was centrifuged at 22,000 × *g* for 20 min. The pellet was resuspended in lysate buffer and centrifuged at 46,000 × *g*. The resultant pellet was resuspended in the lysate buffer as a crude plasma membrane fraction. All procedures were performed at 4 °C.

CHO-K1 cells expressing *Slc26a6* were scraped off dishes 20 h after the transfection and incubated for 30 min in radioimmune precipitation assay buffer (Thermo Fisher Scientific) supplemented with protease inhibitor cocktails. The dissolved cells were spun at 14,000 × *g* for 20 min at 4 °C, and the resultant supernatant was used as whole-cell lysate.

For Western blot analysis, the protein concentrations of the crude plasma membrane from salivary glands and whole-lysate from *Slc26a6*-transfected CHO-K1 cells were determined using the bicinchoninic acid method (Thermo Fisher Scientific), separated in 4–12% SDS-PAGE BisTris gels, and transferred to a polyvinylidene difluoride membrane using the iBlot 2 Dry blotting system according to the manufacturer's instructions (Thermo Fisher Scientific). The transferred membrane was blocked for 1 h at 20 °C in 5% dry milk (Bio-Rad) in Tris-buffered saline supplemented with 0.1% Tween 20 (TTBS) and then incubated with mouse monoclonal anti-SLC26A6 antibody (Santa Cruz Biotechnology) at 1:100 overnight at 4 °C or with peroxidase-conjugated mouse monoclonal anti-β-actin antibody (Sigma) at 1: 25,000 for 1 h at room temperature. Following three washes with TTBS, the membrane was incubated with rabbit peroxidase-conjugated anti-mouse antibody at 1:1000 for 1 h at room temperature. The signal was developed using Femto SuperSignal according to the manufacturer's instructions (Thermo Fisher Scientific), and images were acquired using ImageJ software. For the glycosidase treatment, *N*-linked glycosylated proteins were digested with PNGaseF

according to the manufacturer's denaturing protocol (New England Bio-Rad).

Immunohistochemistry

PGs, SMGs, and SLGs from *Slc26a6*$^{+/+}$ and *Slc26a6*$^{-/-}$ mice were fixed with 4% paraformaldehyde and paraffin-embedded as described previously (47). The 5-μm-thick sections were deparaffinized and rehydrated and, before immunostaining, underwent antigen retrieval in Tris-EDTA–buffered saline (pH 9.0) for 10 min with a pressure cooker. Sections were blocked in 20% donkey serum for 30 min at room temperature and incubated with rabbit anti-Slc26a6 antibody (11) at 1:50, rat anti-Cftr antibody (CFTR Folding Consortium) at 1:100, and goat anti-NKCC1 antibody (Santa Cruz Biotechnology) at 1:100 overnight at 4 °C. For the secondary antibody, donkey anti-rabbit (Alexa 647,), donkey anti-rat (Alexa 488), and donkey anti-goat (Alexa 555) were applied in 1:200, 1:200, and 1:400 dilutions, respectively (Invitrogen). Slides were mounted with Fluoroshield^{TM} containing 4′,6-diamidino-2-phenylindole and visualized on a Nikon A1R+ confocal microscope with a Plan Fluor ×40/1.3 numerical aperture oil immersion objective.

Cell culture and transfections

CHO-K1 cells (Sigma-Aldrich) were maintained as described previously (48). Plasmids encoding *Mus musculus Slc26a6* (GenBank accession no. NM_134420), *Slc4a2* (Ae2, GenBank accession no. BC_054102), *Slc4a9* (Ae4, GenBank accession no. NM-172830.2), and pCMV-Entry as an empty vector control were obtained from OriGene. Cells were electroporated (Nucleofector II, Amaxa) with 6 μg of each plasmid along with 6 μg of pmax GFP (Amaxa) using Nucleofector kit V (Lonza) according to the manufacturer's instructions and seeded onto 5-mm-diameter coverslips (Warner Instrument). Exchanger activity was determined 18–20 h after electroporation in cells that co-expressed GFP signal.

Mouse submandibular gland acinar cell isolation

Submandibular glands were surgically removed and enzymatically dispersed as before (47). Briefly, cells were incubated in BME containing 1.0 mg/ml collagenase 2 (Worthington) and digested by two steps of 25-min incubation each at 37 °C with continuous gassing with 95% O_2 and 5% CO_2.

Intracellular Cl^- and pH measurements

Salivary gland acinar cells were loaded with the Cl^--sensitive dye 6-methoxy-*N*-(3-sulfopropyl) quinolimium (SPQ, 5 mM) for 25 min during the second collagenase digestion step. After dispersion and dye loading, acinar cells were rinsed and resuspended in 5 ml of BME at 37 °C. Plasmid-transfected CHO-K1 cells were loaded with SPQ using a hypotonic loading buffer, as described previously (48). In brief, cells attached to a coverglass were incubated in a 150 mOsm hypotonic solution containing 5 mM SPQ for 4 min at 23 °C.

Cells loaded with the Cl^--sensitive dye SPQ were transferred to a perfusion chamber mounted on the stage of an inverted microscope (Nikon, Eclipse TE 300) equipped with an Optoscan Imaging System (CAIRN Instruments) coupled to a digital CMOS camera (Hamamatsu, C11440). SPQ fluorescence was excited at 340 nm, and emissions were collected at 510 nm.

Anion exchanger activity was monitored in GFP-positive CHO-K1 cells and isolated SMG acinar cells using the following solutions: for Cl^-/oxalate exchanger activity, oxalate-containing, high Cl^- solution composed of 4.3 mM KCl, 95 mM NaCl, 27 mM NMDG-Cl, 5 mM glucose, 10 mM HEPES, 1 mM $MgCl_2$, and 25 mM Na_2 oxalate; and oxalate-containing, low Cl^- solution composed of 4.3 mM potassium gluconate, 95 mM sodium gluconate, 2 mM NMDG-Cl, 25 mM mannitol, 5 mM glucose, 10 mM HEPES, 1 mM $MgCl_2$, and 25 mM Na_2 oxalate. The solution pH and osmolality were adjusted to 7.4 and 300–310 mOsm H_2O/kg with UltraPure Tris (Invitrogen) and sucrose, respectively.

Mouse salivary gland acinar cells express three distinct types of Cl^- flux pathways, including Tmem16a Ca^{2+}-activated chloride channels, Nkcc1 $Na^+/K^+/2Cl^-$ cotransporters, and the anion exchangers Ae2, Ae4, and Slc26a6. Consequently, the following strategy was designed to isolate Slc26a6-mediated Cl^-/oxalate anion exchange in isolated acinar cells. First, SPQ-loaded acinar cells were simultaneously depleted of intracellular Cl^- and loaded with oxalate by exposure to a low Cl^- (4 mM), oxalate-containing (25 mM) solution and then returned to a high Cl^- (153.3 mM), oxalate-free solution (Na_2 oxalate was replaced with NaCl) to induce Cl^-/oxalate anion exchange in the presence of 10 μM T16Ainh-A01, 80 μM bumetanide, and 30 μM EZA to inhibit Tmem16a, Nkcc1, and carbonic anhydrases, respectively. All solutions were HCO_3^--free and gassed with 100% O_2 to prevent Cl^-/HCO_3^- exchanger activity.

The intracellular pH of isolated SMG acinar cells was monitored as described previously (35). Briefly, cells were incubated with 2 μM BCECF/AM for 15 min at 37 °C in an incubator gassed with 95% O_2 and 5% CO_2. Cl^-/HCO_3^- exchange activity was induced in BCECF-loaded SMG cells by exposure to a low Cl^- solution. Solutions were as follows. High Cl^- solution (B+) contained 4.3 mM KCl, 120 mM NaCl, 25 mM $NaHCO_3^-$, 5 mM glucose, 10 mM HEPES, 1 mM $CaCl_2$, and 1 mM $MgCl_2$. Low Cl^- solution contained 4.3 mM potassium gluconate, 120 mM sodium gluconate, 25 mM $NaHCO_3^-$, 5 mM glucose, 10 mM HEPES, 1 mM $CaCl_2$, and 1 mM $MgCl_2$. HCO_3^--containing solutions were gassed with 95% O_2, 5% CO_2 for at least 30 min. The HCO_3^--free, high Cl^- and HCO_3^--free, low Cl^--solutions (B−) were made by substituting $NaHCO_3^-$ with NaCl or sodium gluconate, respectively. The HCO_3^--free solutions were gassed with 100% O_2. Solutions had a pH level of 7.4. The initial rates of Cl^- uptake and intracellular alkalization were estimated from the linear portion of the $[Cl^-]_i$ and pH_i increases divided by the corresponding time periods (~40 s) and expressed as the Cl^- uptake and alkalization rates ($10^{-3}s^{-1}$), respectively.

Ex vivo perfusion of submandibular glands

Mice were anesthetized by intraperitoneal injection of chloral hydrate (400 mg/kg of body weight), and the SMG was surgically removed for *ex vivo* perfusion as described previously (49). Briefly, the isolated SMG was transferred to a perfusion chamber and perfused at 37 °C through the common carotid artery with experimental solutions. Salivation was induced by addition of a β-adrenergic agonist (isoproterenol, 1.0 μM), and

the flow rate and total amount of collected saliva were measured by recording the progression of saliva through a capillary tube at 1-min intervals. The secreted saliva was stored at −20 °C until further analysis. The bicarbonate-containing perfusion solution was composed of 4.3 mM KCl, 120 mM NaCl, 25 mM $NaHCO_3^-$, 5 mM glucose, 10 mM HEPES, 1 mM $CaCl_2$, and 1 mM $MgCl_2$ (pH 7.4, gassed with 95% O_2/5% CO_2). The oxalate-containing solution was the same as the bicarbonate-containing solution with the addition of 1 mM Na_2Oxalate.

Ion composition of saliva

The HCO_3^- concentration in saliva was determined using a colorimetric assay as described by the manufacturer (Diazyme Laboratories, DZ122A-K). Oxalate concentration in saliva was measured using a colorimetric oxalate assay kit (Abnova) and plate reader (Bio-Rad, model 680). The colorimetric oxalate assay results were confirmed by ion exchange chromatography (Proteomics and Mass Spectrometry Facility, Danforth Plant Science Center).

Statistical analysis

Results are presented as the mean ± S.E. Statistical significance was determined using Student's *t* test or one-way ANOVA followed by Bonferroni's *post hoc* test for multiple comparisons (Origin 7.0 Software, OriginLab, Northampton, MA). *p* values of less than 0.05 were considered statistically significant. Experiments were performed using preparations from three or more mice for each condition. For RNA sequencing analysis (12), the FPKM values acquired from the three major salivary glands were compared using one-way ANOVA followed by Bonferroni's *post hoc* test, and $p < 0.05$ was considered to be statistically significantly different.

Author contributions—T. Mukaibo, A. T. G., D. T. T., X. G., C. M., G. E. S., M. S., and J. E. M. conceptualization; T. Mukaibo, T. Munemasa, A. T. G., D. T. T., X. G., and J. E. M. formal analysis; T. Mukaibo and J. E. M. validation; T. Mukaibo, T. Munemasa, A. T. G., D. T. T., J. H., G. E. S., M. S., and J. E. M. investigation; T. Mukaibo, T. Munemasa, D. T. T., X. G., and J. E. M. visualization; T. Mukaibo, T. Munemasa, A. T. G., D. T. T., X. G., J. H., C. M., G. E. S., M. S., and J. E. M. methodology; T. Mukaibo, X. G., and J. E. M. writing-original draft; T. Mukaibo and J. E. M. project administration; T. Mukaibo, T. Munemasa, A. T. G., D. T. T., X. G., J. H., C. M., G. E. S., M. S., and J. E. M. writing-review and editing; X. G. and J. E. M. data curation; X. G. software; J. E. M. resources; J. E. M. supervision; J. E. M. funding acquisition.

Acknowledgments—We thank Yasna Jaramillo and Jaideep Honavar for technical assistance and Dr. Keitaro Satoh for generous advice regarding protein isolation. The Veterinary Research Core was supported by Core Grant 1-ZIG-DE000740 from the NIDCR, National Institutes of Health.

References

1. Alper, S. L., and Sharma, A. K. (2013) The SLC26 gene family of anion transporters and channels. *Mol. Aspects Med.* **34,** 494–515 CrossRefCrossRef Medline Medline
2. Jiang, Z., Grichtchenko, I. I., Boron, W. F., and Aronson, P. S. (2002) Specificity of anion exchange mediated by mouse Slc26a6. *J. Biol. Chem.* **277,** 33963–33967 CrossRef Medline
3. Whittamore, J. M., and Hatch, M. (2017) Loss of the anion exchanger DRA (Slc26a3), or PAT1 (Slc26a6), alters sulfate transport by the distal ileum and overall sulfate homeostasis. *Am. J. Physiol. Gastrointest. Liver Physiol.* **313,** G166–G179 CrossRef Medline
4. Xie, Q., Welch, R., Mercado, A., Romero, M. F., and Mount, D. B. (2002) Molecular characterization of the murine Slc26a6 anion exchanger: functional comparison with Slc26a1. *Am. J. Physiol. Renal Physiol.* **283,** F826–F838 CrossRef Medline
5. Knauf, F., Yang, C. L., Thomson, R. B., Mentone, S. A., Giebisch, G., and Aronson, P. S. (2001) Identification of a chloride-formate exchanger expressed on the brush border membrane of renal proximal tubule cells. *Proc. Natl. Acad. Sci. U.S.A.* **98,** 9425–9430 CrossRef Medline
6. Chernova, M. N., Jiang, L., Friedman, D. J., Darman, R. B., Lohi, H., Kere, J., Vandorpe, D. H., and Alper, S. L. (2005) Functional comparison of mouse slc26a6 anion exchanger with human SLC26A6 polypeptide variants: differences in anion selectivity, regulation, and electrogenicity. *J. Biol. Chem.* **280,** 8564–8580 CrossRef Medline
7. Ko, S. B., Zeng, W., Dorwart, M. R., Luo, X., Kim, K. H., Millen, L., Goto, H., Naruse, S., Soyombo, A., Thomas, P. J., and Muallem, S. (2004) Gating of CFTR by the STAS domain of SLC26 transporters. *Nat. Cell Biol.* **6,** 343–350 CrossRef Medline
8. Ohana, E., Shcheynikov, N., Moe, O. W., and Muallem, S. (2013) SLC26A6 and NaDC-1 transporters interact to regulate oxalate and citrate homeostasis. *J. Am. Soc. Nephrol.* **24,** 1617–1626 CrossRef Medline
9. Dorwart, M. R., Shcheynikov, N., Yang, D., and Muallem, S. (2008) The solute carrier 26 family of proteins in epithelial ion transport. *Physiology* **23,** 104–114 CrossRef Medline
10. Lohi, H., Lamprecht, G., Markovich, D., Heil, A., Kujala, M., Seidler, U., and Kere, J. (2003) Isoforms of SLC26A6 mediate anion transport and have functional PDZ interaction domains. *Am. J. Physiol. Cell Physiol.* **284,** C769–C779 CrossRef Medline
11. Wang, Z., Petrovic, S., Mann, E., and Soleimani, M. (2002) Identification of an apical Cl^-/HCO_3^- exchanger in the small intestine. *Am. J. Physiol. Gastrointest. Liver Physiol.* **282,** G573–G579 CrossRef Medline
12. Gao, X., Oei, M. S., Ovitt, C. E., Sincan, M., and Melvin, J. E. (2018) Transcriptional profiling reveals gland-specific differential expression in the three major salivary glands of the adult mouse. *Physiol. Genomics* CrossRef Medline
13. Wang, Y., Soyombo, A. A., Shcheynikov, N., Zeng, W., Dorwart, M., Marino, C. R., Thomas, P. J., and Muallem, S. (2006) Slc26a6 regulates CFTR activity *in vivo* to determine pancreatic duct HCO_3^- secretion: relevance to cystic fibrosis. *EMBO J.* **25,** 5049–5057 CrossRef Medline
14. Aronson, P. S. (2006) Essential roles of CFEX-mediated Cl^--oxalate exchange in proximal tubule NaCl transport and prevention of urolithiasis. *Kidney Int.* **70,** 1207–1213 CrossRef Medline
15. Aronson, P. S. (2010) Role of SLC26A6-mediated Cl^--oxalate exchange in renal physiology and pathophysiology. *J. Nephrol.* **23,** S158-S164 Medline
16. Freel, R. W., Hatch, M., Green, M., and Soleimani, M. (2006) Ileal oxalate absorption and urinary oxalate excretion are enhanced in Slc26a6 null mice. *Am. J. Physiol. Gastrointest. Liver Physiol.* **290,** G719–G728 CrossRef Medline
17. Soleimani, M., and Xu, J. (2006) SLC26 chloride/base exchangers in the kidney in health and disease. *Semin. Nephrol.* **26,** 375–385 CrossRef Medline
18. Corbetta, S., Eller-Vainicher, C., Frigerio, M., Valaperta, R., Costa, E., Vicentini, L., Baccarelli, A., Beck-Peccoz, P., and Spada, A. (2009) Analysis of the 206M polymorphic variant of the SLC26A6 gene encoding a Cl^- oxalate transporter in patients with primary hyperparathyroidism. *Eur. J. Endocrinol.* **160,** 283–288 Medline
19. Jiang, Z., Asplin, J. R., Evan, A. P., Rajendran, V. M., Velazquez, H., Nottoli, T. P., Binder, H. J., and Aronson, P. S. (2006) Calcium oxalate urolithiasis in mice lacking anion transporter Slc26a6. *Nat. Genet.* **38,** 474–478 CrossRef Medline
20. Monico, C. G., Weinstein, A., Jiang, Z., Rohlinger, A. L., Cogal, A. G., Bjornson, B. B., Olson, J. B., Bergstralh, E. J., Milliner, D. S., and Aronson, P. S. (2008) Phenotypic and functional analysis of human SLC26A6 variants in patients with familial hyperoxaluria and calcium oxalate nephrolithiasis. *Am. J. Kidney Dis.* **52,** 1096–1103 CrossRef Medline

21. Ishiguro, H., Namkung, W., Yamamoto, A., Wang, Z., Worrell, R. T., Xu, J., Lee, M. G., and Soleimani, M. (2007) Effect of Slc26a6 deletion on apical Cl^-/HCO_3^- exchanger activity and cAMP-stimulated bicarbonate secretion in pancreatic duct. *Am. J. Physiol. Gastrointest. Liver Physiol.* **292,** G447–G455 CrossRef Medline
22. Lee, M. G., Ohana, E., Park, H. W., Yang, D., and Muallem, S. (2012) Molecular mechanism of pancreatic and salivary gland fluid and HCO_3^- secretion. *Physiol. Rev.* **92,** 39–74 CrossRef Medline
23. Park, H. W., and Lee, M. G. (2012) Transepithelial bicarbonate secretion: lessons from the pancreas. *Cold Spring Harb. Perspect. Med.* **2,** a009571 CrossRef Medline
24. Stewart, A. K., Yamamoto, A., Nakakuki, M., Kondo, T., Alper, S. L., and Ishiguro, H. (2009) Functional coupling of apical Cl^-/HCO_3^- exchange with CFTR in stimulated HCO_3^- secretion by guinea pig interlobular pancreatic duct. *Am. J. Physiol. Gastrointest. Liver Physiol.* **296,** G1307–G1317 CrossRef Medline
25. Taher, A. A. (1989) The incidence and composition of salivary stones (sialolithiasis) in Iran: analysis of 95 cases–a short report. *Singapore Dent. J.* **14,** 33–35 Medline
26. Yamamoto, H., Sakae, T., Takagi, M., Otake, S., and Hirai, G. (1983) Weddellite in submandibular gland calculus. *J. Dent. Res.* **62,** 16–19 CrossRef Medline
27. Thomson, R. B., Thomson, C. L., and Aronson, P. S. (2016) *N*-glycosylation critically regulates function of oxalate transporter SLC26A6. *Am. J. Physiol. Cell Physiol.* **311,** C866–C873 CrossRef Medline
28. Aebi, M. (2013) *N*-linked protein glycosylation in the ER. *Biochim. Biophys. Acta* **1833,** 2430–2437 CrossRef Medline
29. Lohi, H., Kujala, M., Kerkelä, E., Saarialho-Kere, U., Kestilä, M., and Kere, J. (2000) Mapping of five new putative anion transporter genes in human and characterization of SLC26A6, a candidate gene for pancreatic anion exchanger. *Genomics* **70,** 102–112 CrossRef Medline
30. Petrovic, S., Ma, L., Wang, Z., and Soleimani, M. (2003) Identification of an apical Cl^-/HCO_3^- exchanger in rat kidney proximal tubule. *Am. J. Physiol. Cell Physiol.* **285,** C608–C617 CrossRef Medline
31. Simpson, J. E., Schweinfest, C. W., Shull, G. E., Gawenis, L. R., Walker, N. M., Boyle, K. T., Soleimani, M., and Clarke, L. L. (2007) PAT-1 (Slc26a6) is the predominant apical membrane Cl^-/HCO_3^- exchanger in the upper villous epithelium of the murine duodenum. *Am. J. Physiol. Gastrointest. Liver Physiol.* **292,** G1079–G1088 CrossRef Medline
32. Sindić, A., Chang, M. H., Mount, D. B., and Romero, M. F. (2007) Renal physiology of SLC26 anion exchangers. *Curr. Opin. Nephrol. Hypertens.* **16,** 484–490 CrossRef Medline
33. Song, Y., Yamamoto, A., Steward, M. C., Ko, S. B., Stewart, A. K., Soleimani, M., Liu, B. C., Kondo, T., Jin, C. X., and Ishiguro, H. (2012) Deletion of Slc26a6 alters the stoichiometry of apical Cl^-/HCO_3^- exchange in mouse pancreatic duct. *Am. J. Physiol. Cell Physiol.* **303,** C815–C824 CrossRef Medline
34. Gonzalez-Begne, M., Nakamoto, T., Nguyen, H. V., Stewart, A. K., Alper, S. L., and Melvin, J. E. (2007) Enhanced formation of a HCO_3^- transport metabolon in exocrine cells of $Nhe1^{-/-}$ mice. *J. Biol. Chem.* **282,** 35125–35132 CrossRef Medline
35. Peña-Münzenmayer, G., Catalán, M. A., Kondo, Y., Jaramillo, Y., Liu, F., Shull, G. E., and Melvin, J. E. (2015) Ae4 (Slc4a9) anion exchanger drives Cl^- uptake-dependent fluid secretion by mouse submandibular gland acinar cells. *J. Biol. Chem.* **290,** 10677–10688 CrossRef Medline
36. Shcheynikov, N., Yang, D., Wang, Y., Zeng, W., Karniski, L. P., So, I., Wall, S. M., and Muallem, S. (2008) The Slc26a4 transporter functions as an electroneutral $Cl^-/I^-/HCO_3^-$ exchanger: role of Slc26a4 and Slc26a6 in I^- and HCO_3^- secretion and in regulation of CFTR in the parotid duct. *J. Physiol.* **586,** 3813–3824 CrossRef Medline
37. Hong, J. H., Park, S., Shcheynikov, N., and Muallem, S. (2014) Mechanism and synergism in epithelial fluid and electrolyte secretion. *Pflugers Arch.* **466,** 1487–1499 CrossRef Medline
38. Park, S., Shcheynikov, N., Hong, J. H., Zheng, C., Suh, S. H., Kawaai, K., Ando, H., Mizutani, A., Abe, T., Kiyonari, H., Seki, G., Yule, D., Mikoshiba, K., and Muallem, S. (2013) Irbit mediates synergy between Ca^{2+} and cAMP signaling pathways during epithelial transport in mice. *Gastroenterology* **145,** 232–241 CrossRef Medline
39. Wang, Z., Wang, T., Petrovic, S., Tuo, B., Riederer, B., Barone, S., Lorenz, J. N., Seidler, U., Aronson, P. S., and Soleimani, M. (2005) Renal and intestinal transport defects in Slc26a6-null mice. *Am. J. Physiol. Cell Physiol.* **288,** C957–C965 CrossRef Medline
40. Aronson, P. S. (2002) Ion exchangers mediating NaCl transport in the renal proximal tubule. *Cell Biochem. Biophys.* **36,** 147–153 CrossRef Medline
41. Singh, A. K., Sjoblom, M., Zheng, W., Krabbenhoft, A., Riederer, B., Rausch, B., Manns, M. P., Soleimani, M., and Seidler, U. (2008) CFTR and its key role in *in vivo* resting and luminal acid-induced duodenal HCO_3^- secretion. *Acta Physiol. (Oxf.)* **193,** 357–365 CrossRef Medline
42. Lustmann, J., Regev, E., and Melamed, Y. (1990) Sialolithiasis: a survey on 245 patients and a review of the literature. *Int. J. Oral Maxillofac. Surg.* **19,** 135–138 CrossRef Medline
43. Wu, C. C., Hung, S. H., Lin, H. C., Lee, C. Z., Lee, H. C., and Chung, S. D. (2016) Sialolithiasis is associated with nephrolithiasis: a case-control study. *Acta Otolaryngol.* **136,** 497–500 CrossRef Medline
44. Wahl, R., and Kallee, E. (1994) Oxalic acid in saliva, teeth and tooth tartar. *Eur. J. Clin. Chem. Clin. Biochem.* **32,** 821–825 Medline
45. Poole, D. F., and Tyler, J. E. (1970) Oxalic acid-produced surface phenomena on human enamel examined by scanning electron microscopy. *Arch. Oral Biol.* **15,** 1157–1162 CrossRef Medline
46. Romanenko, V. G., Catalán, M. A., Brown, D. A., Putzier, I., Hartzell, H. C., Marmorstein, A. D., Gonzalez-Begne, M., Rock, J. R., Harfe, B. D., and Melvin, J. E. (2010) Tmem16A encodes the Ca^{2+}-activated Cl^- channel in mouse submandibular salivary gland acinar cells. *J. Biol. Chem.* **285,** 12990–13001 CrossRef Medline
47. Catalán, M. A., Kondo, Y., Peña-Munzenmayer, G., Jaramillo, Y., Liu, F., Choi, S., Crandall, E., Borok, Z., Flodby, P., Shull, G. E., and Melvin, J. E. (2015) A fluid secretion pathway unmasked by acinar-specific Tmem16A gene ablation in the adult mouse salivary gland. *Proc. Natl. Acad. Sci. U.S.A.* **112,** 2263–2268 CrossRef Medline
48. Peña-Münzenmayer, G., George, A. T., Shull, G. E., Melvin, J. E., and Catalán,M.A.(2016)Ae4(Slc4a9)isanelectroneutralmonovalentcation-dependent Cl^-/HCO_3^- exchanger. *J. Gen. Physiol.* **147,** 423–436 CrossRef Medline
49. Romanenko, V. G., Nakamoto, T., Srivastava, A., Begenisich, T., and Melvin, J. E. (2007) Regulation of membrane potential and fluid secretion by Ca^{2+}-activated K+ channels in mouse submandibular glands. *J. Physiol.* **581,** 801–817 CrossRef Medline